Journal Pre-proofs

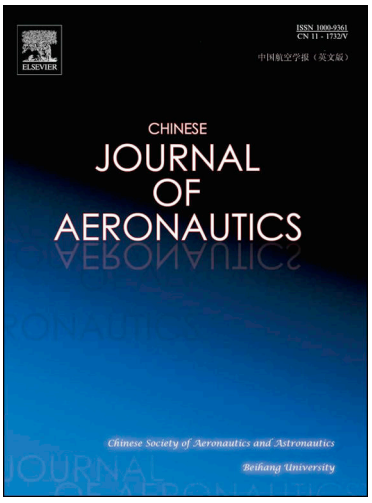

Deep learning enabled localization for UAV autolanding

Minghui Li, Tianjiang Hu

PII: S1000-9361(20)30564-1
DOI: https://doi.org/10.1016/j.cja.2020.11.011
Reference: CJA 1883

To appear in: *Chinese Journal of Aeronautics*

Received Date: 29 May 2020
Revised Date: 8 November 2020
Accepted Date: 8 November 2020

Please cite this article as: M. Li, T. Hu, Deep learning enabled localization for UAV autolanding, *Chinese Journal of Aeronautics* (2021), doi: https://doi.org/10.1016/j.cja.2020.11.011

Chinese Journal of Aeronautics 28 (2015) xx-xx

Contents lists available at ScienceDirect

Chinese Journal of Aeronautics

journal homepage: www.elsevier.com/locate/cja

Final Accepted Version

Deep learning enabled localization for UAV autolanding

Minghui LI , Tianjiang HU *

Machine Intelligence and Collective RObotics (MICRO) Lab, Sun Yet-sen University, Guangzhou 510275, China

Received 29 May 2020; revised 26 July 2020; accepted 16 October 2020

Abstract

This article concentrates on ground vision guided autonomous landing of a fixed-wing Unmanned Aerial Vehicle (UAV) within Global Navigation Satellite System (GNSS) denied environments. Cascaded deep learning models are developed and employed into image detection and its accuracy promoting for UAV autolanding, respectively. Firstly, we design a target bounding box detection network BboxLocate-Net to extract its image coordinate of the flying object. Secondly, the detected coordinate is fused into spatial localization with an extended Kalman filter estimator. Thirdly, a point regression network PointRefine-Net is developed for promoting detection accuracy once the flying vehicle's motion continuity is checked unacceptable. The proposed approach definitely accomplishes the closed-loop mutual inspection of spatial positioning and image detection, and automatically improves the inaccurate coordinates within a certain range. Experimental results demonstrate and verify that our method outperforms the previous works in terms of accuracy, robustness and real-time criterions. Specifically, the newly developed BboxLocate-Net attaches over 500 fps, almost five times the published state-of-the-art in this field, with comparable localization accuracy.

Keywords: UAV autolanding; Stereo Vision; Safe Landing; Deep Learning; Localization

E-mail address: hutj3@mail.sysu.edu.cn

1. Introduction

In the past few decades, Unmanned Aerial Vehicles (UAVs) have drawn more and more research attention due to their remarkable characteristics, such as low risk of casualties, low cost, lightweight, and great mobility associated with adaptability to dirty, dull and/or dangerous situations. UAVs have, therefore, been applied to a variety of scenarios, including meteorological detection, local area monitoring, survey and mapping, forest fire prevention, earthquake rescue[1] and many more. With the integration of advanced automation technology, unmanned vehicles can perform regular-cruise tasks with quite little manual intervention, since the task workspace is almost wide when the vehicle is flying in the air. However, take-off and/or landing is still a technological challenge because the vehicle works in a quite compact space that has complicated relationship with the ground. Specifically, landing of the fixed-wing vehicles has been proven to be the most challenging and hazardous period of aerial flight in many practical applications.[2] Even minor errors in guidance or control might cause system damages or even crashes. This situation becomes more remarkable due to a variety of complex application scenarios and meteorological environment conditions. Under such circumstances, autonomous landing has been an important and essential technique for unmanned systems within unknown or Global Navigation Satellite System (GNSS)-denied scenarios.[3] Hereafter, autonomous landing within GNSS-denied scenarios is called as autolanding. Furthermore, this article concentrates on vision-based localization for autolanding then.

Previous research on vision-guided autonomous UAV landing can be categorized into onboard vision and ground vision modes. The onboard vision mode usually employs one or more cameras installed on the flying vehicle as a positioning sensor.[4-7] When the aerial vehicle approaches the ground runway, the

camera detects the runway and plans an appropriate landing trajectory. In contrast, the ground vision mode distributes and fixes vision systems on the ground.[8- 10]

Compared with onboard navigators, the ground vision system possesses more scalable computing resources and can save costs by placing them on a runway instead of configuring each vehicle separately. Furthermore, the image from the ground-to-air perspective is much more convenient for processing than the images from the air-to-ground view. Therefore, in this study, we focus on the ground vision mode for autolanding of fixed-wing unmanned aircraft.

So far, several prototypes of ground vision based autonomous landing systems have been developed in Refs.[8-10], respectively. All are concerned with a mapping from image sequences to spatial trajectories using computer vision which usually involves two workflow steps: flying vehicle target detection and automatic positioning. In this study, the vision automatic detection schemes are concerned and considered further. As for similar scenarios, Yang et al.[8] presented accurate UAV landing performance in a GPS-denied environment, by running a ground-based near infrared camera system. A nose infrared laser lamp is fixed on the vehicle as a cooperative marker for image detection. The foreground area of the candidate targets is obtained by a simple morphological pre-processing. Researchers at Portuguese Navy Research Center[9] used a ground based monocular vision system supporting the autonomous landing of a fixed-wing aerial vehicle onto a fast patrol boat. For obtaining the relative pose of the vehicle, they employed several 3D model-based system combinations using the Computer-Aided Design (CAD) model for tracking. Both systems need to know the geometrical model or place the cooperative marker on the flying vehicle. On the contrary, Kong et al. developed a traditional stereo ground-based system including two pan-tilt units and two cameras, without relying on any cooperative onboard marker or geometrical knowledge.[10] Since the system was conducted, Hu et al.[3,10,11] have been working on algorithms of automatic detection and localization on an autolanding vehicle. Both corner-based and skeleton-based algorithms have been designed and implemented to target detection on the ground captured sequential images.[3,12] Tang et al. [3] initially integrated the active contour method into Chan-Vese model detection, and an extended Kalman estimator was developed for ground vision based localization. Thanks to on-ground sufficient computing resources, Cao et al.[13] adopted and improved a flying vehicle tracking algorithm based on GOTURN, which attaches the frame rate to 100 fps, nearly 5 times higher than that of the Chan-Vese algorithm.

Although the pre-existing researches have shown remarkable detection performance in the UAV autolanding processing, challenges still exist in accuracy, robustness and real-time feature. Yang's target detection method[8] is only suitable for UAVs equipped with infrared laser lamp at the nose, which is difficult to be generalized for various types of aircraft. Due to the processing rate of below 25 fps, the real-time performance of Chan-Vese is seldom appropriate for practical applications of autolanding.[3] Similarly, the GOTURN tracking based method[13] relies on human-computer interaction for labeling the bounding box within the first frame. Meanwhile, the tracking error ought to accumulate for a long-term period. Once a frame is tracked to the fall target, it may cause inefficacy of the whole vision-based tracking even. Particularly, some scenarios cannot be correctly treated by using the pre-existing methods. For instance, part of the landing vehicle goes out of the field of view, and only the partial body is captured from the images.

In the consideration of the existing issues in ground vision based methods, this paper innovatively investigates a novel deep learning-based method that maps sequential image frames into the spatial localization of UAVs at the autolanding period. Deep learning supports a higher processing speed of target detection, and enables a greater accuracy promotion of vision-based positioning further. The overall algorithm has a great improvement in accuracy, robustness and real-time performance in comparison with the prior works. The contributions of this paper are summarized as follows:

(1) A light-weight convolutional deep neural network model, namely BboxLocate-Net, is proposed and implemented to perform an initial coarse prediction on spatial coordinates of the landing aircraft. The proposed BboxLocate-Net model solves the too-many-parameters-tuning problem existing in classic object detection deep networks and achieves a practical and effective balance between speed and accuracy.

(2) A spatial motion continuity criterion is defined and fused into quantitative checking on the landing target detection, by taking full advantage of the high-speed rate of the light-weight detection network.

(3) A key point regression network, namely PointRefine-Net, is developed to promote localization accuracy in the case that the flying vehicle's motion continuity is checked unacceptable. Then, the self-correction of error detection is realized, and both robustness and accuracy are improved simultaneously.

2. Ground vision for UAV autolanding

Aimed at runway taxiing and landing of medium aerial vehicles, a ground stereo vision-based system has been developed and updated for several times.[10,14-18] Previous several corresponding mapping

algorithms to produce the spatial trajectory of the landing vehicle have also be testified via online experiments supported by the on-ground vision system.[3,10,12,13] Here, we will review the ground vision system deployment and the overall workflow for the ground-to-air visual system.

2.1 System architecture and deployment

The ground stereo vision-based system usually works in the aircraft descending and taxing stages to guide it moving in the field of view to accomplish automatic landing. It usually consists of four modules: image capture module, target detection module, position calculation module and data transmission module.[3,10] In the image capture module, two binocular cameras are symmetrically installed on the independent Pan-Tilt Units (PTUs) to capture the landing sequential images. Each PTU with camera module works independently and has two degrees of freedom to expand the search scope. Each PTU is controlled, serves to track the landing target, and feeds the pitching and yawing angles backward. The target detection module and position calculation module are used for 2D image target detection and 3D spatial location calculation, respectively. Both of them run on the same ground image processing computer. The data transmission module transmits the calculated spatial coordinates onto the onboard autopilot via wireless data link. A general deployment scheme has been designed and implemented for ground stereo guidance prototypes, as shown in Fig. 1.

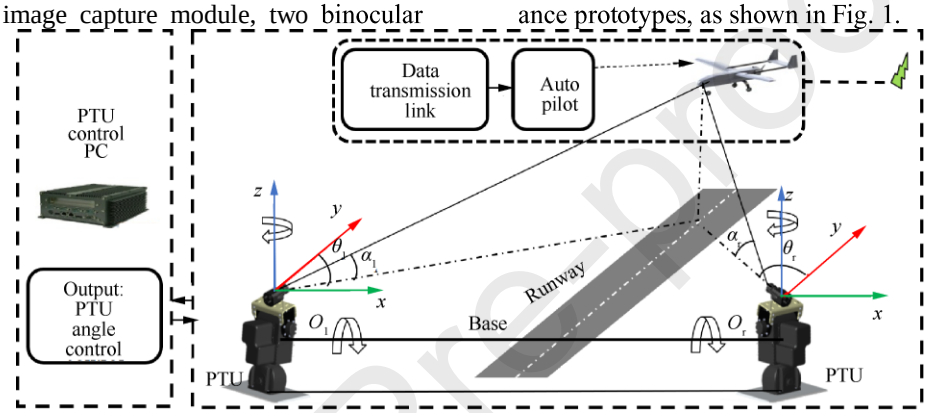

(a) General configuration and deployment of developed ground vision system

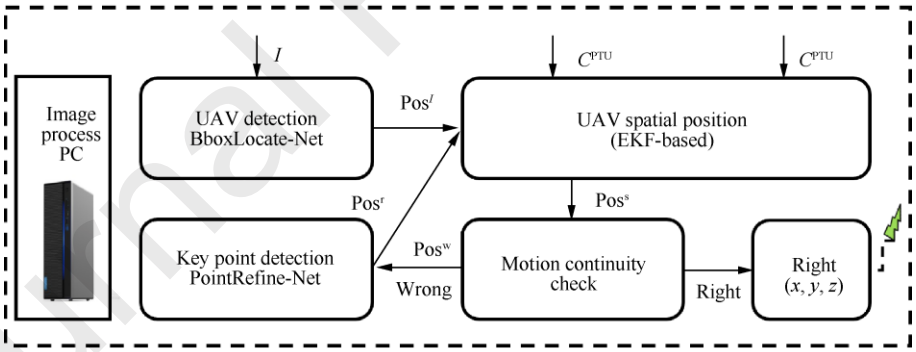

(b) Overall workflow of developed algorithm models from sequential images into spatial trajectory

Fig. 1 Schematic diagram of ground stereo system for autonomous landing of the fixed-wing aerial vehicle.

In real-scenario flights, a fixed-wing unmanned aircraft is guided into the view of the stereo camera by its onboard navigation system. Once the target is detected, the ground-based guidance system switches from the waiting state to the working mode. Two cameras capture the vehicle landing images, and then, the captured sequential images and PTU parameters are transferred to the image processing computer which detects the key point of the flight target and calculates its spatial coordinates. Finally, the spatial coordinates are wirelessly transmitted onto the onboard autopilot to facilitate autonomous landing.

In terms of deployment details, we assume that the origin of the world coordinate system (x, y, z) is at the rotation center of the left PTU, from the practical viewpoint of the published works [3,10,13]. The axis of the camera frame is parallel to that of the PTU frame in the initial position. The right camera is mounted on the x axis, with the light center of the left and right cameras represented as O_l and O_r, respectively. The baseline of the optical system is O_lO_r. θ_l, θ_r, α_l and α_r respectively represent the tilt and pan angles. The anticlockwise measurement is positive. At the same time, the

hardware configuration is updated to be compatibl e with the deep learning requirements. The captur ed image is transferred to the high-performance c omputing platform instead of the original control computer. The GPU component performs high-loa d computations for flight target detection in seque ntial images, while the CPU is responsible for inf ormation-based positioning and wireless data trans mission.

2.2 Overall workflow of vision-based localization

The ground stereo vision-based localization algorit hm outputs the aircraft spatial coordinates during its autolanding process, while captured sequential images and camera attitudes are inputted online. Generally speaking, the overall workflow is comp osed of image-based target detection and filter-bas ed localization.

On the basis of the system described in Section 2.1, the previous positioning algorithms have been developed and verified within simulation and experimental scenarios.[3] The landing vehicle's spatial coordinates are directly mapped by using the stereo measurement model, once knowing the target coordinates of the left as well as right images and the PTU attitude parameters. In details, it assumes that the UAV actual coordinate is (x_w, y_w, z_w), and its coordinate on the left and right image plane is (u_l, v_l) and (u_r, v_r), respectively. f is the focal length of the camera. d_x and d_y are the pixel sizes in X and Y directions. $\boldsymbol{R}^L$ and $\boldsymbol{R}^R$ represent the rotation matrix of the world coordinate system relative to the left and right camera coordinate systems respectively. Then, the relationship of the coordinate between the 3D world and 2D image plane is calculated by

$$\begin{bmatrix} u_l \\ v_l \\ 1 \end{bmatrix} = \frac{1}{z_c} \cdot \begin{bmatrix} f/d_x & 0 & u_0 & 0 \\ 0 & f/d_x & v_0 & 0 \\ 0 & 0 & 1 & 0 \end{bmatrix} \begin{bmatrix} \boldsymbol{R}^L & \boldsymbol{T}^L \\ \boldsymbol{0}^T & \boldsymbol{1} \end{bmatrix} \begin{bmatrix} x_w \\ y_w \\ z_w \\ 1 \end{bmatrix} \tag{1}$$

$$\begin{bmatrix} u_r \\ v_r \\ 1 \end{bmatrix} = \frac{1}{z_c} \cdot \begin{bmatrix} f/d_x & 0 & u_0 & 0 \\ 0 & f/d_x & v_0 & 0 \\ 0 & 0 & 1 & 0 \end{bmatrix} \begin{bmatrix} \boldsymbol{R}^R & \boldsymbol{T}^R \\ \boldsymbol{0}^T & \boldsymbol{1} \end{bmatrix} \begin{bmatrix} x_w \\ y_w \\ z_w \\ 1 \end{bmatrix} \tag{2}$$

$$\begin{cases} u_l = f_{ul}(x_w, y_w, z_w, \alpha_l, \theta_l) \\ v_l = f_{vl}(x_w, y_w, z_w, \alpha_l, \theta_l) \\ u_r = f_{ur}(x_w, y_w, z_w, \alpha_r, \theta_r) \\ v_r = f_{vr}(x_w, y_w, z_w, \alpha_r, \theta_r) \end{cases} \tag{3}$$

The stereo vision algorithm processes the spatial coordinates one point by one point, so random disturbance is inevitably involved in the outputted trajectory under the mentioned principle of triangulation. Tang et al.[3] proposed an extended Kalman filter estimator to improve localization accuracy by fusing knowledge of aircraft motion continuity. Here, $\boldsymbol{X}$= [x_w, y_w, z_w, v_x, v_y, v_z] ^{T} denotes state variables, and $\boldsymbol{Y}$= [u_l, v_l, u_r, v_r] ^{T} means the observation values of detected target coordinates in images. By constructing the state observation equation Eq. (4) and the state estimation equation Eq. (5), the whole system state estimation process is completed through five recursive steps of extended Kalman filter. Real-scenario flight experiments have demonstrated that this method is more robust and accurate than the triangulation-based localization algorithm.[3]

$$\begin{cases} \hat{\boldsymbol{X}}_{(k|k-1)} = \boldsymbol{F}\hat{\boldsymbol{X}}_{(k-1|k-1)} + \boldsymbol{\Gamma W} \\ \hat{\boldsymbol{Y}}_{(k-1|k-1)} = \boldsymbol{h}_k\left(\hat{\boldsymbol{X}}_{(k-1|k-1)}\right) + \boldsymbol{V}_k \end{cases} \tag{4}$$

$$\boldsymbol{Y}_{(k|k-1)} = \boldsymbol{h}_k\left(\hat{\boldsymbol{X}}_{(k-1|k-1)}\right) = \begin{bmatrix} u_l \\ v_l \\ u_r \\ v_r \end{bmatrix} = \begin{bmatrix} f_{ul}\left(x_w, y_w, z_w, v_x v_y, v_z\right) \\ f_{vl}\left(x_w, y_w, z_w, v_x, v_y, v_z\right) \\ f_{ur}\left(x_w, y_w, z_w, v_x, v_y, v_z\right) \\ f_v\left(x_w, y_w, z_w, v_x, v_y, v_z\right) \end{bmatrix} \tag{5}$$

where $\boldsymbol{F}$ is a state transition matrix. $\boldsymbol{W}_k$ and $\boldsymbol{V}_k$ represent the system process noise and the observation noise respectively. $\boldsymbol{\Gamma}$ is the gain of the process noise. $\boldsymbol{h}_k$ is the measurement matrix. $\hat{\boldsymbol{X}}_{(k|k-1)}$ denotes the result predicted by the previous state. $\hat{\boldsymbol{X}}_{(k-1|k-1)}$ is the optimal result of the previous state. $\hat{\boldsymbol{Y}}_{(k-1|k-1)}$ means the optimal observation value of the previous state.

Eventually, this article employs deep learning models into a fast and accurate detection on the autolanding sequential images, since the pre-existing works need to be promoted with the processing rate and localization accuracy. Specifically, the proposed approach will be an original trial for the challenging scenario when the landing aircraft is partially out of the field of view.

3. Deep learning models enabling accurate and fast detection

In this study, a cascaded deep learning model is proposed and developed to enable ground vision based autolanding, with considerations on the existing challenges of real-time and accuracy. Such a scheme takes full advantage of the scalability of computing resources supported by the ground vision system. Firstly, the ground stereo mode is flexibly extendable to computing and/or storage resources. Here, we upgrade the computing platform to GTX1080ti to run the deep learning algorithm more efficiently. Secondly, annotated mixed landing datasets are conducted through a large number of actual and simulation flight experiments. Hereafter, two lightweight learning networks are developed to enable a fast and accurate detection on the autolanding vehicle. Such a hierarchical structure processes vision-based localization

from coarse extraction to fine correction. Thirdly, the system scalability is both feasible and effective for improving the real-time and accuracy of the ground stereo guidance system. Finally, higher processing speed provides extra operations of motion continuity checking and coordinate correction for autolanding localization. Furthermore, the proposed two-hierarchy deep neural models are implemented, demonstrated and validated as well.

3.1. Two-hierarchy architecture of cascaded deep neural networks

A cascaded two-hierarchy convolution network is employed to make fast coarse-to-fine prediction. In the first hierarchy, we propose a bounding box regression-based convolutional network, whose input is the complete image captured by the camera. It is mainly responsible for predicting the aircraft ROI (Region-Of-Interest) coordinates in the whole image, and assuming the center point of the bounding box as the key point location. The second-hierarchy network takes the local ROI predicted by the first-hierarchy network as input, allowing only a certain range of modifications to the former coarse predictions. The inputted image size and search range keep decreasing along the cascade.

The detected bounding box certainly contains or covers the landing aircraft, but mismatching does exist between the detected box's center and the actual image coordinates in either horizontal or vertical direction. Such mismatching phenomenon often results in localization inaccuracy of the landing vehicle. It is even worse to lead to failure of the visual positioning task. Hereafter, we introduce a second-level network to optimize the accuracy of the vision-based localization algorithm. Under such two-hierarchy architecture, the first level aims to estimate key point position robustly with few considerable errors, while the second level is designed to produce higher accuracy.

The proposed cascaded deep learning detection method consists of four stages, as shown in Fig.2. In details, BboxLocate-Net represents the first-level network, and PointRefine-Net represents the second-level network. In the first stage, an autolanding image dataset with annotations is conducted to train the coarse detection model BboxLocate-Net. It is followed by a PointRefine-Net training process which takes lots of random small areas including key points as samples. In the third stage, the captured UAV image is detected by BboxLocate-Net. In the fourth stage, the bounding box produced by the BboxLocate-Net detection module is finally used by the point refinement module PointRefine-Net to obtain a more accurate estimation of the guiding target.

In Sections 3.2 and 3.3, we will focus on the deep neural network structure and algorithm workflow of each hierarchy. The combining strategies of cascaded two-level networks will be presented in Section 3.4.

3.2. Deep learning based target detection

The goal of detection algorithm is to locate and classify the targets during the UAV autolanding process. The detected objects are usually labeled with bounding boxes, category information and confidence score as well.

Recently, there have been more and more researches on object detection. Faster R-CNN, [19] the two-stage proposal-driven CNN object detector, reaches great accuracy on many challenging datasets, while the processing speed is still a major concern. Facts show that Faster R-CNN is seldom an optimal solution for real-time flying vehicle detection. YOLO v3, [20] the one-stage detector, not only demonstrates promising results but also yields about 10 times faster detection speed. Experimental results demonstrate that its accuracy reduces by about 12% compared to Faster R-CNN, and it still can hardly achieve real-time detection in the autolanding scenarios.

Considering the balance between accuracy and processing time, this paper proposes a novel UAV object detection network named BboxLocate-Net which is designed to create a smaller-scale, faster, and more efficient deep neural model. Without increasing the network depth and width, we address this issue from a different perspective. Using DenseNet[21] as a reference, we exploit the potential of the network through feature reuse and multi-scale fusion, and combine BboxLocate-Net as a feature extractor and YOLOv3 predictor. The BboxLocate-Net algorithm training and testing process are shown in Fig.2.

We design BboxLocate-Net's architecture based on the several principles of improving the real-time capacity and accuracy simultaneously. At first, reducing the network parameters is the key to improve the real-time performance. It is inspired by the DenseNet[21] network to enhance the feature reuse between layers, full use shallow and deep information, and reduce the number of parameters. The proposed network introduces a dense connection from one layer to all subsequent layers, developing a highly dense feature reuse connection among the five-layer feature maps. Different from DenseNet,[21] we cascade the feature maps as the decreasing order of their resolution. In this study, it is named as "Ladder-Dense" connection.

Then, the network is further designed to improve the detection accuracy. When the landing vehicle approaches and descends, the target is usually small and the background is relatively complex. The small target in the deep low-resolution feature map tends to be lost. To guarantee the accuracy of small-scale target

detection, an HRNet[22] inspired approach is adopted to make full use of the information across all scales of the image, and reduce the loss of feature maps information due to the decrease of image resolution. Such an HRNet-inspired network works with a high-resolution subnetwork as the first parallel path, and gradually adds the other low-resolution layer's resolution-hold parallel path one by one. As a result, the parallel path explores the network potential while maintaining resolution. In the output part of the network, a multi-scale fusion unit is deployed to cascade the information from all parallel subnetworks[21] to capture and integrate information at all scales of an image.

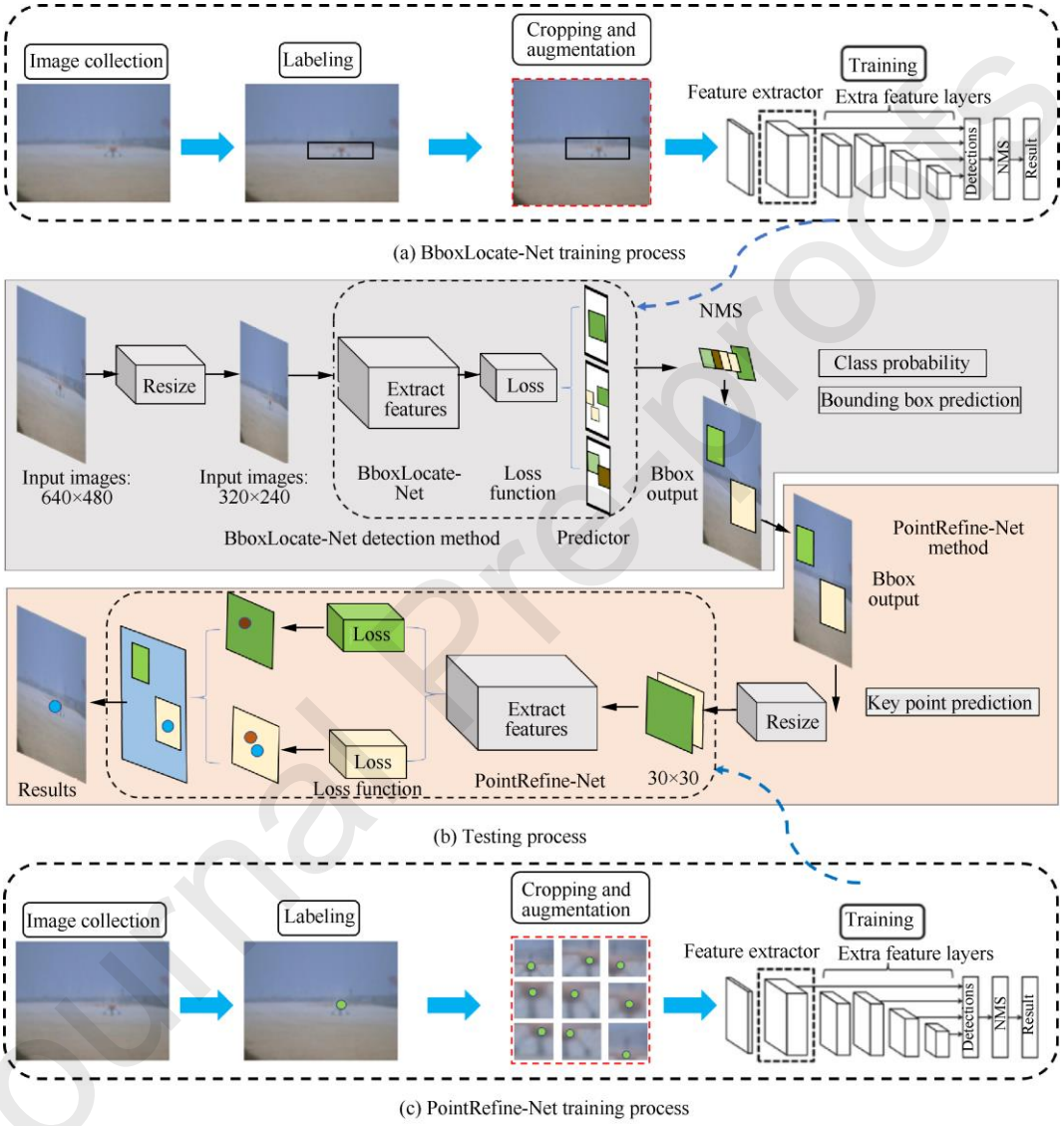

Fig. 2 Structure of detection model based on BboxLocate-Net and PointRefine-Net.

Finally, considering the real-time performance and accuracy of the detection network, the proposed BboxLocate-Net is tested with excellent performance in specified datasets. It has been noted that HRNet and DenseNet, two state-of-the-art networks, have produced excellent performance in large-scale dataset detection tasks such as COCO[23], ImageNet[24] and VOC[25]. Specifically, the autolanding image datasets have only two classes of plane and background. The proposed BboxLocate-Net rightly achieves a balance between prediction accuracy and processing speed, by combining the advantages of DenseNet and HRNet together.

During the detection process, each image captured from the ground cameras is resized to 320×240 to match BboxLocate-Net. Then, the 20×15×18 prediction tensor is automatically generated through the feature extraction network BboxLocate-Net and the YOLO detection layer. Each of the 1×1×30 tensor includes the target location information: center coordinates (x, y), width w, height h, category information

and confidence score c.[20] After obtaining the confidence c of each prediction box, a threshold will be set to remove the boxes with a score below. Then the remaining bounding boxes are filtered with the non-maximal suppression to obtain multiple sets of high-score bounding boxes. In particular, the YOLOv3 predictor uses a set of initial anchor boxes with fixed width and height to regress and predict the target position. Here, K-means clustering[26] is adopted to determine the number and the best size of anchor boxes. As shown in Fig.3, three clustering centers are presented for the training dataset using K-means clustering. The yellow box and the blue box respectively represent two benchmark anchor boxes with different sizes. The final red box predicted by BboxLocate-Net is calculated based on three anchor boxes.

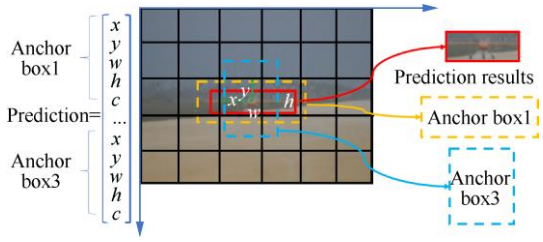

Fig. 3 Detection results based on multiple anchor boxes.

The kernel task of the BboxLocate-Net network is to calculate the object confidence value, while prediction on the width, height and central coordinates of the UAV target is concerned as well. For example, Loss values of aircraft detection generally include head frame coordinate loss $\text{Loss}_{\text{coor}}$ and confidence loss $\text{Loss}_{\text{conf}}$. The calculation equation is as follows:

$$\text{Loss(UAV)} = \text{Loss}_{\text{coor}} + \text{Loss}_{\text{conf}} \tag{6}$$

On one hand, $\text{Loss}_{\text{coor}}$ is quantitatively analyzed by

$$\begin{aligned}\text{Loss}_{\text{coor}} = {} & \lambda_{\text{coord}} \sum_{i=0}^{S^2} \sum_{j=0}^{B} I_{ij}^{\text{obj}} \left[\left(x_i - \hat{x}_i\right)^2 + \left(y_i - \hat{y}_i\right)^2 \right] + \\ & \lambda_{\text{coord}} \sum_{i=0}^{S^2} \sum_{j=0}^{B} I_{ij}^{\text{obj}} \left[\left(\sqrt{w_i} - \sqrt{\hat{w}_i}\right)^2 + \left(\sqrt{h_i} - \sqrt{\hat{h}_i}\right)^2 \right]\end{aligned} \tag{7}$$

where I_{ij}^{obj} denotes the possibility of a landing target in the j th anchor box of the i th grid; λ_{coord} is the weight of positioning error, generally equal to 5; x_i, y_i, w_i and h_i represent the UAV bounding box coordinates, width and height which are detected in the i th grid, respectively; $\hat{x}_i$, $\hat{y}_i$, $\hat{w}_i$ and $\hat{h}_i$ mean actual position parameters from training data of the i th grid; S^2 represents the total number of grids after passing through the network; B is the number of anchor boxes.

On the other hand, the loss function of confidence $\text{Loss}_{\text{conf}}$ is quantified as

$$\text{Loss}_{\text{conf}} = \sum_{i=0}^{S^2} \sum_{j=0}^{B} I_{ij}^{\text{obj}} \left[\left(C_i - \hat{C}_i\right)^2 \right] + \lambda_{\text{noobj}} \sum_{i=0}^{S^2} \sum_{j=0}^{B} I_{ij}^{\text{noobj}} \left[\left(C_i - \hat{C}_i\right)^2 \right] \tag{8}$$

where λ_{noobj} denotes the weight coefficient of confidence error; C_i indicates the confidence of the target contained in the i th grid of all S^2 grids; $\hat{C}_i$ represents the confidence parameter of the i th grid in the manually labeled data.

3.3. Deep learning based accuracy promoting

In the previous works of ground vision based autolanding, the detection rate of frames is not fast enough, so there is no extra time to make corrections or refinement to errors in the detection.[3,13] In this paper, we propose a second-level point regression network to further optimize the target's image coordinates. The above mentioned BboxLocate-Net greatly optimizes the speed of UAV target detection and provides the possibility for the implementation of motion continuity check and coordinate correction.

For practical applications, a criterion for checking the motion continuity is necessary to determine whether or not to conduct an accuracy promoting algorithm. In this paper, we synthesize the distance and angle indexes into the motion continuity criterion. We define F (x_i, y_i) as the candidate point. P (x_1, y_1) and Q (x_2, y_2) denote the last two points of the UAV trajectory, and $|FQ|$ denotes the space distance between point F and point Q. Then when the following two conditions are satisfied at the same time, F is regarded as correct. Otherwise, it is confirmed to be mismatched and has to be corrected, so we have the following equation:

$$|FQ| = \sqrt{(x_i - x_2)^2 + (y_i - y_2)^2 + (z_i - z_2)^2} \le 1.5\,|PQ| \tag{9}$$

$$\angle PQF \ge 120^{\circ} \tag{10}$$

Then, once the output of the first-level network is checked as not acceptably continuous, the second-level point regression network PointRefine-Net starts to run. PointRefine-Net is a key point regression network that is responsible for correcting the key point coordinates in a small ROI. The training samples are 9 small areas with different sizes and positions randomly captured near the key points of each picture. The network is mainly used to optimize the offset value (x, y) of the key point from the upper left corner of the area. In order to minimize the loss of key point coordinate offset, the convolution kernel parameters are updated iteratively by using the backward gradient propagation algorithm. When the loss value is less than the threshold value 0.002, the network stops training and we get the final point regression network model. Fig. 2(c) shows the training process of the PointRefine-Net.

The PointRefine-Net's architecture is designed in the attempt to improving the real-time capacity and detection accuracy. Since the input of the second-level network is only a small part of the original image, we design a resolution preserving point regression network. The feature extraction network is basically the same as the sequential path part of BboxLocate-Net. However, the difference between them is that the resolution of the first few layers changes from high to

low in BboxLocate-Net but stays the same in PointRefine-Net. In the shallow layers, for encouraging feature reuse, the front layer of feature extraction network of PointRefine-Net uses dense connection. In the deep layers, to effectively process and consolidate features across scales, we choose to use a single pipeline with skip layers to preserve spatial information at each resolution which is proposed in Hourglass. [27]

Finally, the first five layers of PointRefine-Net are connected with Dense-connection, and the output part with Hourglass-connection[27]. Based on the structure, PointRefine-Net becomes a simple, minimal deep learning detection network that has the capacity to capture all of these features and bring them together to output pixel-wise predictions.

In the process of key point detection, the input of PointRefine-Net is an inaccurate bounding box containing UAV target detected by BboxLocate-Net network. After the image resolution is resized to 30 × 30, the convolution operation is carried out. The output tensor only contains the key point coordinate information (x, y). Fig.4 shows the optimization process of PointRefine-Net from the inaccurate bounding box detected by BboxLocate-Net to the accurate point. The red dot is a wrong detection result. The green dot indicates the corrected result.

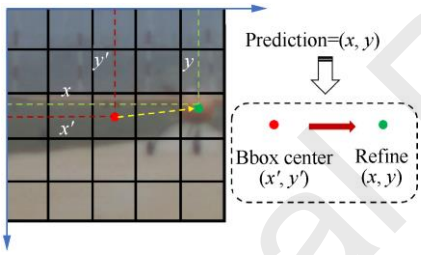

Fig. 4 Schematic diagram of error coordinate correction.

The single task of PointRefine-Net network is to predict the key point coordinate vector. For a UAV head key point, Eq. (11) is the loss function of the head key point regression task.

$$\text{Loss}=\sum_{i=0}^{S^2}\sum_{j=0}^{B} I_{ij}^{\text{obj}}\left[(x_i-\hat{x}_i)^2+(y_i-\hat{y}_i)^2\right] \tag{11}$$

where x_i and y_i represent the center coordinates of the predicted i th grid; $\hat{x}_i$ and $\hat{y}_i$ stand for actual position parameters from training data of the i th grid.

3.4. Vision-based localization algorithm and workf low

Combining with Section 2.2 and the detailed desc ription of the cascaded detection models, we are r eady to present our overall localization algorithm flowchart. When actually detecting the UAV targe t, first, the BboxLocate-Net network receives the complete image and predicts the bounding box co ordinate of the UAV target. Then, combining with PTUs parameters, we calculate the UAV spatial position based on EKF-based object spatial localiz ation algorithm[3] and check the motion continuity. If the coordinate is identified as an error point, w e take the local ROI predicted by the BboxLocate -Net as the input of second-level network. Finally, PointRefine-Net can precisely correct the key poi nt coordinates in this ROI. The details are shown in Table 1.

4. Cascaded deep learning model based detecti on experiment

To evaluate the performance of the proposed novel target detection method, we compare the image detection results with the trajectory data collected in flight experiments. The data were obtained in a large number of UAV landing mixed images generated by a simulation platform and a real flight experimental platform. In addition, we design the following two groups of experiments to compare the proposed model with other classical detection algorithms in terms of real-time performance and detection accuracy.

(1) The first experiment verifies the accuracy and real-time performance of BboxLocate-Net by comparing it with several classical deep learning target detection algorithms.

(2) The second experiment analyses the detection accuracy of PointRefine-Net and BboxLocate-Net, and proves that the second level network has certain optimization ability for the results detected by first level network.

4.1. Dataset and evaluation protocol

Our previous research has successfully carried out several experiments under normal weather conditions.[3,10,13] To meet the requirements on learning samples, we present an upgraded version of our self-constructed dataset which includes images from our previous dataset and new extracted images captured by the simulation platform. The collection of dataset is divided into two parts: real-scenario image acquisition and simulation-scenario image acquisition. In the past work, a large number of UAV sequential landing images have been captured in the real flight experiments, and several volunteers annotated the sequential images to complete the construction of the real-scenario dataset. The simulation images are mainly collected in the simulation system, namely Airsim, in which we can simulate the whole process of UAV landing on the runway, and can simulate a variety of backgrounds, such as the sky, mountains, forests and so on. Different time conditions such as morning, evening, noon and dusk, and different

weather conditions including sunny, rain and snow can be set under the backgrounds. In the PX4 hardware-in-the-loop simulation system, since the 3D model of UAV is known, we can achieve automatic target labeling by coordinate system transformation. Our new dataset not only contained a larger number of images but also was gathered in more challenging weather conditions (stronger wind smog and heavy snow). The UAV position can also be set up in the distance and attitudes to expand the diversity of data samples. The dataset used in the experiment is an integration of simulated and actual datasets, of which the mixed training dataset consists of actual training dataset and simulated dataset, totaling 13350 pictures. And the mixed validation dataset includes the actual validation dataset and the simulation validation dataset, with a total of 1500 pictures. For real-scenario flight application, we only test our algorithm on the actual flight dataset.

Table 1 UAV target localization method based on cascaded deep learning models.

UAV target localization method based on cascaded deep learning models

Input.
Captured images I
PTU attitudes (yaw, pitch)
UAV dataset with labels M

Output. UAV localization coordinates (x, y, z)

BL-Net and PR-Net training procedure：

for batch in M:
  for X_i in *batch*:
    (1) Obtain the BboxLocate-Net image label：Category C and Bbox coordinate (x, y, w, h), PointRefine-Net image label：key point coordinate (x, y).
    (2) Initializing network parameters and forward propagation.
    while X_i = true do:
      if Loss >= T:
        (A) Backward propagation.
        (B) Gradient descent with momentum.
        (C) Forward propagation, get Loss value.
      else: Save model: obtain the BL-N and PR-N.
    end
  end
end

Test procedure：

Step 1. BboxLocate-Net image object detection.
(A) Resize the captured image resolution to (320,240).
(B) Forward propagation: predict Bbox coordinate (x, y, w, h).
(C) Suppression Bbox of $t_0 < 0.6$.
(D) Non-maximum suppression.
(E) Object detection result：Bbox center (u, v).

Step 2. EKF-based object spatial localization algorithm and motion continuity judgment.
(A) Get positioning result (x, y, z) from（u, v）and PTU attitudes (yaw, pitch).
(B) Motion continuity judgment:
if (x, y, z) is a wrong point：
Go to Step 3：PointRefine-Net receives the key ROI (x, y, w, h).
else:
Return the final positioning value (x, y, z).

Step 3. PointRefine-Net image key point detection.
(A) Resize the captured image resolution to (30, 30).
(B) Forward propagation: predict key point coordinate (u, v).
(C) Get positioning result (x, y, z) with EKF-based localization algorithm and return (x, y, z).

In this section, four evaluation indexes are adopted to evaluate the performance of the cascaded deep learning networks. We use mean Average Precision (mAP) and frames per second (fps) to evaluate the proposed BboxLocate-Net model. And the performance of PointRefine-Net is measured with the average detection error - "Mean Error" and the failure rate of each key point - "False Rate".

The above mentioned two evaluation indexes mAP and FPS both have clear meanings in the target detec-

tion field. We will not define them here. The Mean Error defined in this paper is measured by

$$\text{MeanError} = \frac{\|(u,v)-(\hat{u},\hat{v})\|}{\text{BBox.}_w} \times 100\% \quad (12)$$

where (u, v) and $(\hat{u},\hat{v})$ are the ground truth and the detected position, respectively; BBox._w is the width of the bounding box detected by BboxLocate-Net.

In order to evaluate the accuracy of network prediction results, we define another indicator: False Rate. For the key point detection result of each frame, if the error is larger than 5%, it is considered the detection result of this frame as a failure. This means that the key point position error in each direction cannot be greater than 5% of the target area. In a group of experiments, the key point detection accuracy is defined as the ratio of the number of key points detected failure to the total number of key points.

4.2. BboxLocate-Net and PointRefine-Net training strategy

In this study, we train BboxLocate-Net network based on open source framework Darknet and PointRefine-Net on Caffe. The testing facility is a PC device with 64 GB internal memory and Ubuntu 14.04 operating system, i7-5930K CPU and NVIDIA GeForce GTX 1080ti GPU.

In the training process of BboxLocate-Net, we used a batch size of 64, a momentum of 0.9, and a decay of 0.0005. BN (Batch Normalization) is used to regularize each time the weights are updated. Convolution-layer and pooling operations are used to extract features and generate tensors with specified size. In each forward prediction, the loss function is calculated in the detection layer, and the convolution kernel parameters are updated with the purpose of minimizing the loss value by the backward gradient descent algorithm.

The initialization of PointRefine-Net parameters is the same as that of BboxLocate-Net. Its input image resolution is 30×30, and the batch size is set to 32. We also use small batch random gradient descent to optimize network parameters. The network trains about 150000 times in total, and stops training when the loss value was less than 0.002.

4.3. BboxLocate-Net model based detection experiments

High-precision target detection is the basis of high-precision positioning for stereo vision system. At the same time, the real-time performance of the detection algorithm is also the key factor for the system to be practical.

To make a fair comparison between BboxLocate-Net and other algorithms in real time and accuracy, we have trained all kinds of deep learning methods[20,28-30] under the same conditions. Table 2 summarizes the training parameters that we used for training the UAV detection model. The training details of the network are as follows.

Table 2 Training parameters of five deep learning algorithms.

Algorithm	BboxLocate-Net	YOLOv3	YOLOv3-Tiny	YOLOv2-Tiny	MobileNet-YOLO
Input size (Pixel)	320×240	320×240	320×240	320×240	320×240
Number of epochs	150000	150000	150000	150000	150000
Batch size	64	64	64	64	64
Initial learning rate	0.0001	0.0001	0.0001	0.0001	0.0001
Momentum	0.9	0.9	0.9	0.9	0.9
Decay	0.0005	0.0005	0.0005	0.0005	0.0005
Backbone	BboxLocate-Net	Darknet-53	Darknet-21	Darknet-19	Mobilenets v1

Using mixed landing dataset, we compared the proposed BboxLocate-Net detection results with that obtained by state-of-the-art CNN object detectors such as MobileNets-SSD[29,30], YOLOv2-Tiny[28], YOLOv3[20] and MobileNets-YOLO[20,29]. We use mAP and FPS as comparison indicators for these algorithms. The performance comparison of our algorithm and the existing state-of-the-art approaches is shown in Table 3. Our approach is significantly better than MobileNets-SSD and YOLO v2-Tiny approaches. On the other hand, our tiny network, BboxLocate-Net, achieves an AP of 0.963 and FPS of 503. It outperforms most other algorithms, and is more efficient in terms of model size and computation complexity (GFLOPs). Fig.5 shows the partial detection results of different CNN detection algorithms.

Table 3 Comparison of mAP value and FPS at IoU = 0.5 of different CNN detectors.

Algorithm	Sunny			Rain			Snow			Entire Dataset	Processing rate (fps)
	8:00	12:00	17:00	8:00	12:00	17:00	8:00	12:00	17:00		
BboxLocate-Net	0.96	0.97	0.95	0.96	0.98	0.98	0.97	0.96	0.93	0.963	503
YOLOv3	0.98	0.97	0.94	0.98	0.97	0.95	0.97	0.98	0.95	0.966	31.89
YOLOv3-Tiny	0.93	0.94	0.95	0.91	0.94	0.92	0.94	0.95	0.91	0.932	221
YOLOv2-Tiny	0.91	0.90	0.89	0.89	0.93	0.91	0.92	0.94	0.90	0.910	230
MobileNets-SSD	0.91	0.93	0.92	0.94	0.91	0.92	0.89	0.91	0.94	0.919	289
MobileNets-YOLO	0.89	0.91	0.89	0.91	0.94	0.91	0.92	0.93	0.94	0.916	291

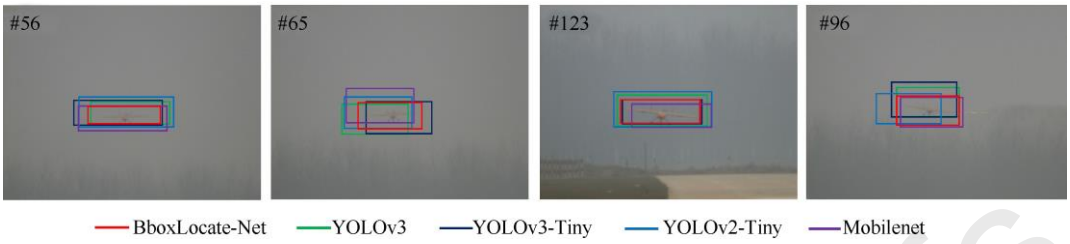

Fig. 5 Test results of different CNN algorithms.

4.4. PointRefine-Net model based detection experiments

For the performance analysis of PointRefine-Net network, we take Mean Error and False Rate as evaluation indexes. In order to test the key point positioning effect in the algorithm, we synthetically analyzed the positioning results of six UAV key points and compared the detection results before and after PointRefine-Net. Fig.6 shows the comparison of the Mean Error and False Rate between PointRefine-Net and BboxLocate-Net when detecting six key points. Compared with BboxLocate-Net, the detection results of PointRefine-Net have improved the accuracy to some extent and can be used as a correcting network for error points. Fig.7 shows the comparison of several detection results before and after PointRefine-Net correction.

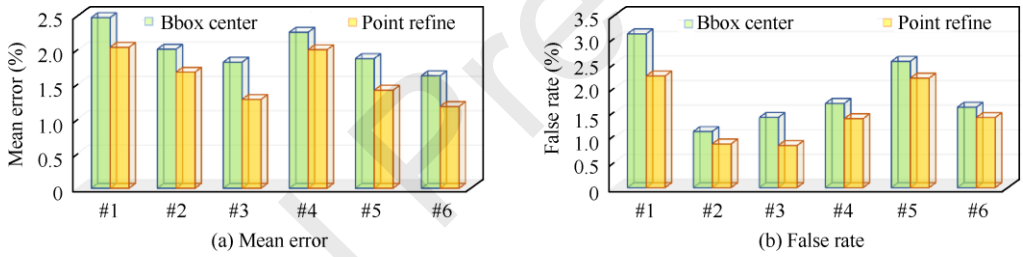

Fig. 6 Comparison of detection results at 6 key points before and after coordinate correction.

Fig. 7 Comparison of key point detection results before and after coordinates correction.

5. Real-scenario flight localization experiments

To comprehensively verify the performance of the algorithm in real-scenario flight, we designed the following two sets of flight experiments using the cascaded deep learning detection algorithm proposed in this paper and the EKF-based localization algorithm[3] as the solving algorithm.

(1) Based on Chan-Vese algorithm, GOTURN algorithm and BboxLocate-Net algorithm, the first group is used to calculate the UAV space trajectory, and to compare the accuracy and real-time capacity.

(2) To prove the better accuracy and robustness of the system after the PointRefine-Net coordinate correction algorithm, the second group mainly compares the influence of PointRefine-Net coordinate correction algorithm and BboxLocate-Net algorithm on the

accuracy and robustness capacity.

5.1. Real-scenario flight localization experiments s etup

The real-scenario flight localization experiments are based on the ground-based visual system mentioned above. The runway baseline is about 10.77 m. The high-precision PTU is set on both sides of the runway and a visible light camera is fixed on the PTU. Each of PTU has two degrees of freedom to expand the search field. At the same time, the high position resolution (0.00625°) and high rotation speed (50 (°)/s) make the positioning more accurate.

Specifically, for visible light camera, we selected the imaging source color CCD high-speed industrial camera, model DFK 23G618, which uses a CCD chip of SonyICX445AQA with a pixel resolution of 640×480, a cell size of 3.2 mm. The lens of the vision system that we adopted is 60 mm. According to the pin-hole camera model, the size of the detection window is 42.67 m×32 m when the depth distance is 800 m. For the medium-sized UAV used in the experiment, the wingspan of the UAV is 2.2 m, and its theoretical imaging pixel at 800 m is 32.99 pixels which can be effectively identified by our CNN model at this distance. The minimum target that our cascaded CNN algorithm can detect is 15 pixels, at which point the corresponding theoretical location distance can be calculated as 1762.5 m. However, because the height of UAV is only about 1/4 of its width, and there is water mist interference and light path consumption in actual use, an experiential guiding distance is set as 800 m. The autolanding experiments are conducted in accordance with such specifications as well.

To extend the field of view, we adopted precision PTU to actuate the camera, which is a two-axis gyro stable turntable from FLIR Corporation of the United States, PTU-D300. The turntable sends commands through a RS232 serial port, and feedbacks its own status online, including the turntable azimuth (pan) and pitch (tilt) angles. Its angle resolution is 0.006°. PTU-D300 is driven by a stepping motor and can meet the requirements of closed-loop tracking targets. The PTU has better vibration and impact resistance, and protection level of IP67. When the UAV flight speed is 30 m/s and the distance from the guidance system is 200 m, the required rotation speed of the turntable is 4.3 (°)/s, which is within the normal working range of the PTU. We installed the camera on the top bracketing, and the assembled individual vision system is illustrated in Fig.1.

Finally, the target detection method mentioned in the paper is used to process the images collected by the two cameras, and then the positioning results are compared with the previous work.

5.2. BboxLocate-Net model based localization exp eriments

(1) Experiment 1.1: Accuracy experiments without PointRefine-Net

Fig.8 shows autonomous landing trajectories and localization errors in *x*, *y* and *z* directions. One trajectory is calculated by EKF-based localization algorithm. The blue trajectory is generated by DGPS as a reference trajectory, and the yellow, light blue and red ones are generated by Chan-Vese, GOTURN and BboxLocate-Net algorithms, respectively.[3,13] The blue area, green area and yellow area in Fig.9 represent three stages of approaching, descending and taxiing in the landing process.

The Root-Mean-Square Error (RMSE) in each axis using EKF is presented in the right of Fig.9. e_x, e_y and e_z denote RMSE in *x*, *y* and *z* directions respectively. For the convenience of display, the error is displayed after taking ln(1+e). The error distribution curves for each axis calculated by EKF at different distances are shown in Fig.10.

In Fig.10，when the *y* coordinate is less than 187 m, the deviation increases rapidly. This is due to the weak DGPS signal when the aircraft approaches the ground.

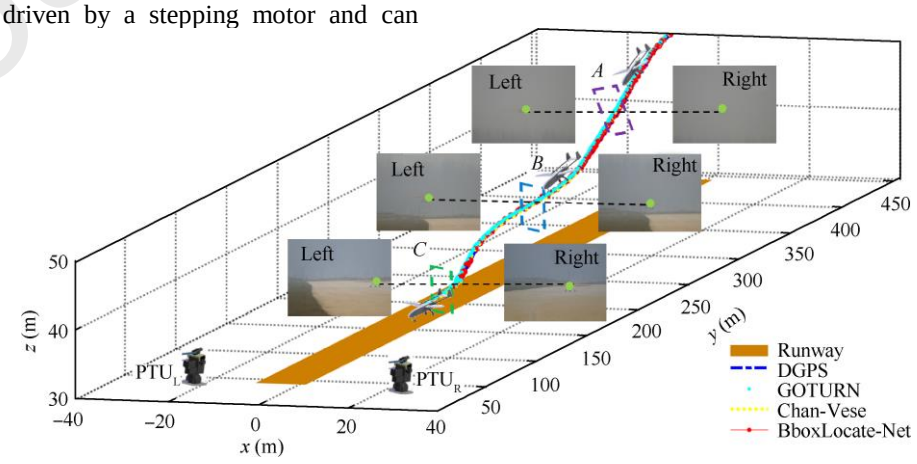

Fig. 8 Localization results using different UAV detection algorithms.

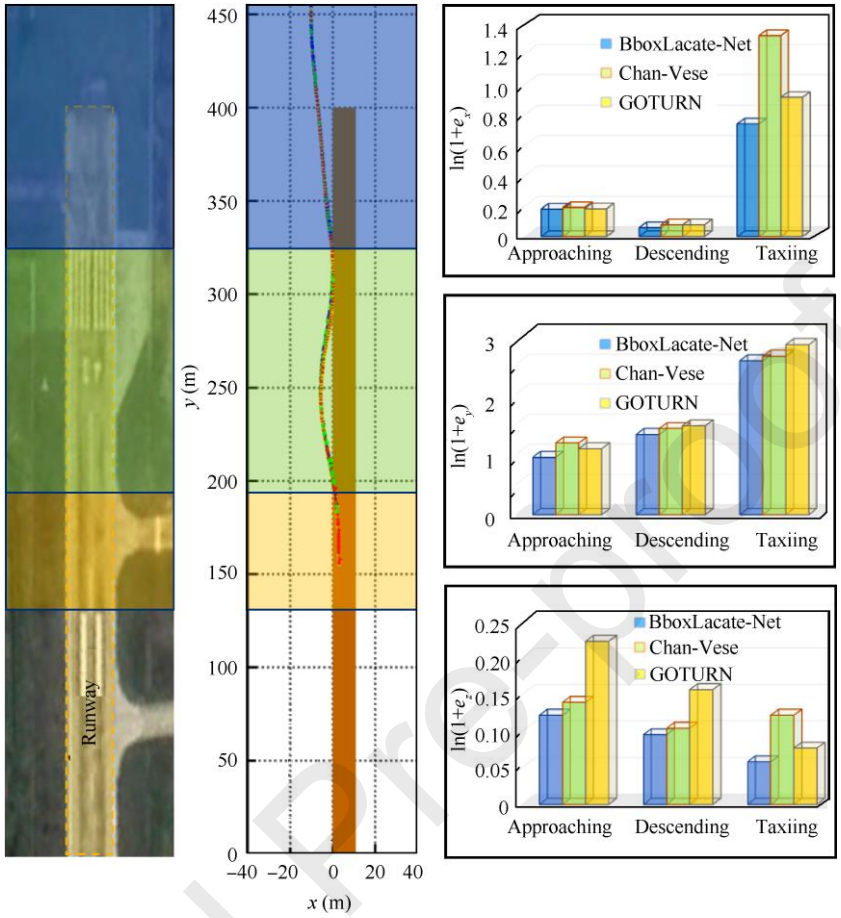

Fig. 9 Accuracy comparison of spatial positioning results.

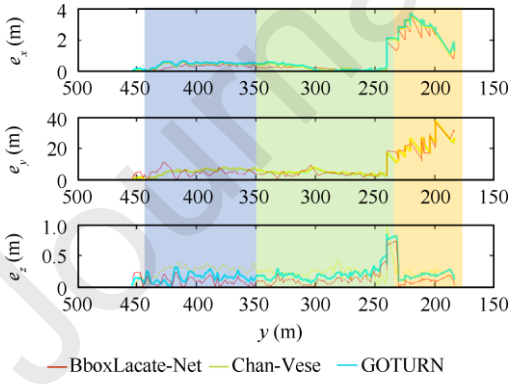

Fig. 10 Localization errors in *x*, *y* and *z* directions for different distance conditions.

By analyzing the two figures together, it is clear that the *y* axis direction error in the three stages is much greater than that in the *x* axis and *z* axis directions. This is due to the error characteristics of binocular vision. Since the *y* axis is parallel to the runway and the runway is long enough, a large *y* axis direction error does not affect the UAV landing process. Relative to *y* axis direction error, *x* and *z* axis direction error are critical for safe landing. Excessive *x* axis direction error may cause the UAV to deviate from the runway, while too large *z* axis direction deviation will cause the UAV to miss the landing point, which is prone to safety accidents. It can be seen in Fig.9 that the error of the *x* axis and *z* axis landing is within 0.3 m in both the stage of approaching and the stage of descending. Only in the taxiing stage, the *x* axis direction error will reach a larger value, which is caused by the binocular calculation characteristics and the image target positioning error. Since the UAV has landed during the taxiing stage, a larger positioning error is acceptable.

According to Fig.9, the BboxLocate-Net localization algorithm reduces the deviation to some extent at all three axes, especially in the “Air&Ground” stage, the trajectory generated by BboxLocate-Net has a smaller deviation than that of Chan-Vese and GOTURN algorithm. To sum up, the localization accuracy improvement owing to BboxLocate-Net localization algorithm is practically significant for UAV autonomous landing.

(2) Experiment 1.2: Real-time capability experiments without PointRefine-Net

The real-time performance of the algorithm has always been a key and common problem in practical engineering applications, and it is also our focus.

We compare the frames per second (fps) of object detection with different algorithms, and these algorithms are tested in the same equipment, which is a PC with i7-5930K CPU and 64 GB internal storage. The results are shown in Table 4. The detection speed of BboxLocate-Net can reach 500 fps, about 500 times of Chan-Vese algorithm and 3 times of GOTURN algorithm. Compared with Chan-Vese algorithm and GOTURN algorithm, our method has great progress in real-time capability.

Table 4 Processing rate with three different detection methods.

Index	Algorithm	Processing rate (fps)
T1	Chan-Vese	10.23±0.8
	GOTURN	172.56±2.42
	BboxLocate-Net	500.23±2.21

5.3. Cascaded deep learning model based localiza tion experiments

(1) Experiment 2.1: Robustness capability experiments with PointRefine-Net

Another trajectory is shown in Fig.11. The image detection results at point *D* and *F* with large deviation in Fig.11 are shown in Figs.12 (a) and (b). It shows that the location error is mainly caused by the wrong image detection results. We conduct PointRefine-Net operation at points *D* and *F*. The light blue dot and yellow dot are the results before and after correction, respectively. And the light blue trajectory and yellow trajectory in Fig.12 respectively represent the positioning results before and after correction. We can see that PointRefine-Net shows better robustness than BboxLocate-Net algorithm.

In Fig.11, the *S* area represents the case that part of the UAV goes out of the field of view. The detection results of four typical frames in *S* area are shown in Fig.13. *G*, *H*, *I* and *J* represent four typical frames which are out of the FOV in *S* area. Purple points are the detection results of Chan-Vese, red points indicate the detection results of GOTURN, and light blue and yellow points indicate the detection results before and after PointRefine-Net network respectively. When the target image coordinates out of the FOV, the comparison of detection results also shows that PointRefine-Net has a more robust performance.

The reason why part of the wing is out of view is that the control accuracy of PTU is unsatisfactory. For analyzing the effect of PTU control accuracy error on spatial positioning, a Monte-Carlo method is used for quantitative evaluation on the effect of PTU control accuracy error on spatial positioning. Eventually, specified artificial servo errors are assumed added to the obtained PTU angles. We analyzed the positioning accuracy after incorporating 1 mrad and 2 mrad error perturbations into the left PTU true values, respectively. When 1 mrad error perturbation is added, the errors in *x*, *y* and *z* direction at several specific distances are shown in Table 5. If 2 mrad error perturbation is added to the left PTU, *x*, *y* and *z* direction errors are shown in Table 6. The analysis results show that there is a large deviation between measurements and the GPS true values in the *y* distance and *z* distance when 2 mrad error is added. When the *y* distance is only 150 m, the height and distance errors are still 0.6 m and 3.176 m respectively, which makes it difficult to guarantee the accurate UAV guidance.

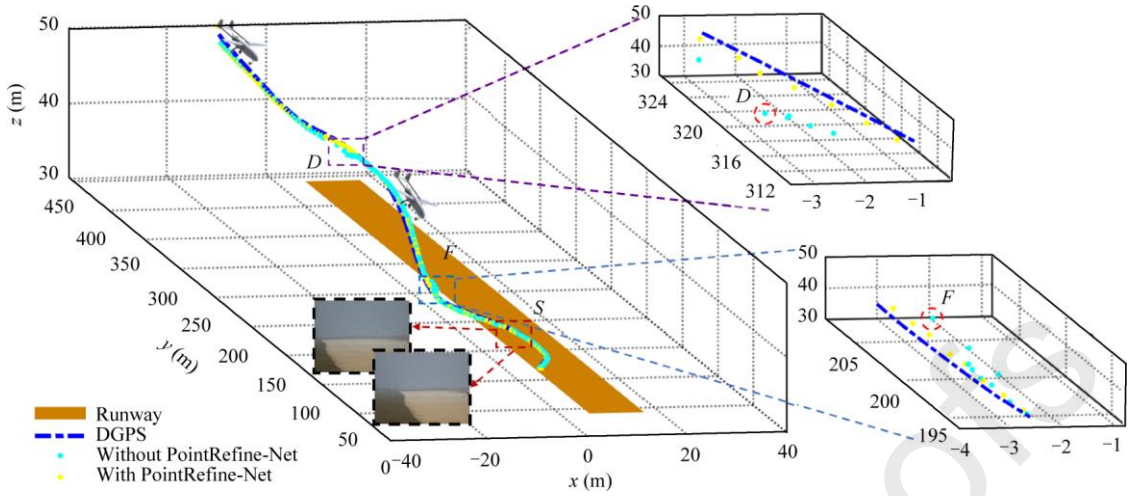

Fig. 11 Comparison of localization results before and after PointRefine-Net.

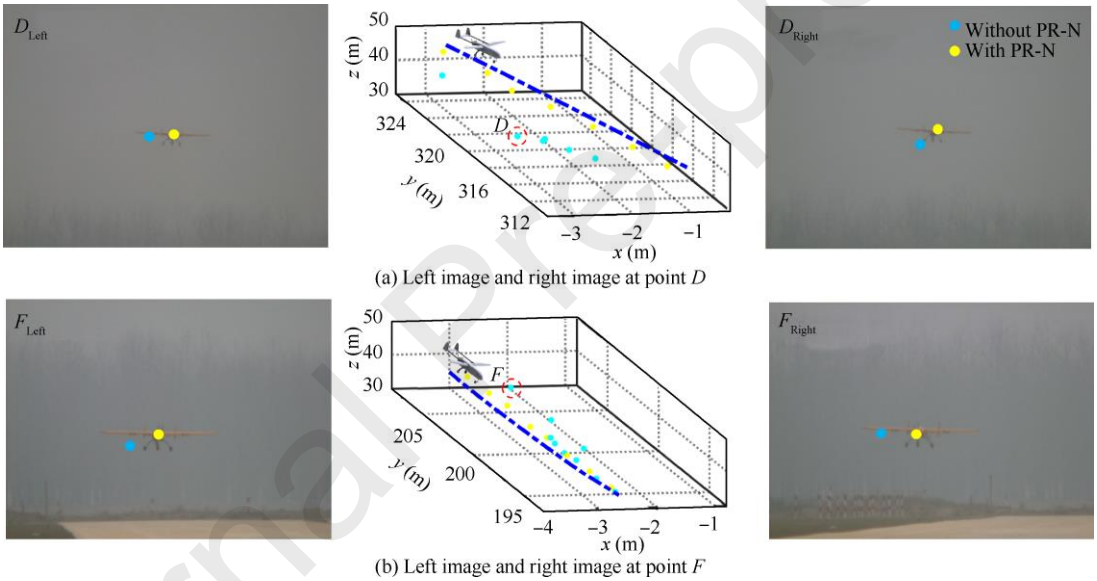

Fig. 12 Comparison of key point detection results before and after PointRefine-Net (PR-N) coordinate correction.

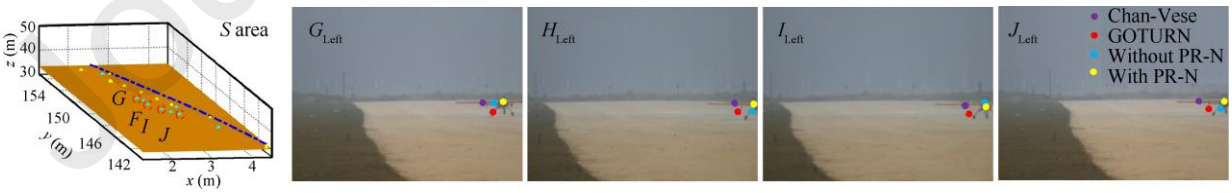

Fig. 13 Key point detection results detected by four detection algorithms.

Table 5 Analysis of positioning error under different *y* distance (1 mrad error perturbation).

y (m)	Measurement error (m)		
	e_x	e_y	e_z
450	0.2152	18.364	1.5429
350	0.1675	9.7402	1.2231

250	0.1060	5.6671	0.5221
150	0.0682	2.3324	0.0653
120	0.0344	2.0611	0.0413

Table 6 Analysis of positioning error under different *y* distance (2 mrad error perturbation).

y (m)	Measurement error (m)		
	e_x	e_y	e_z
450	0.4002	31.095	4.0012
350	0.3298	22.253	3.1073
250	0.2407	11.236	1.6323
150	0.1325	3.1760	0.6425
120	0.0998	3.0421	0.5514

(2) Experiment 2.2: Accuracy experiments with PointRefine-Net

The light blue and yellow trajectories in Fig.11 are generated by different detection algorithms but same localization algorithms. Same as above, blue is generated by DGPS, and light blue and yellow are generated by BboxLocate-Net (BL-N) and PointRefine-Net (PR-N) algorithm, respectively. Table 7 shows the comparison of RMSE with EKF at each axis between the two algorithms in actual landing experiments. It can be seen that the algorithm after PointRefine-Net has higher location accuracy.

We also analyze the spatial positioning accuracy errors caused by detection pixel errors. Fig.14 shows the spatial positioning error changes in each coordinate direction caused by target detection errors (0-30 pixels) in *U* direction and *V* direction of image. We set up three cases of pixel deviation. As shown in Fig.14, the red point indicates that the pixel error increases in the same value in the *U* and *V* directions, the yellow point indicates that the pixel error is constant in the *V* direction and changes in the *U* direction, and the cyan point indicates that the error is constant in the *U* direction and changes in the *V* direction. It is obvious that with the increase of detection error, the *Y* direction error increases the fastest. This is because the baseline of the binocular vision system is much smaller than the distance from the binocular vision system during the UAV landing.

(3) Experiment 2.3: Real-time capability experiments with PointRefine-Net

We use the flight trajectory mentioned in Experiment 2.1 to compare the localization speed before and after PointRefine-Net. The results are shown in Table 7. BboxLocate-Net algorithm has better real-time capability, but PointRefine-Net algorithm has higher location accuracy while the real-time capability is kept in the same level.

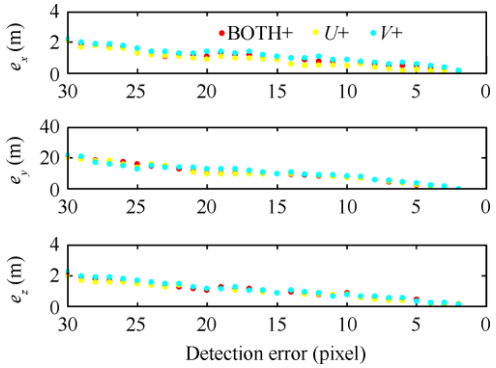

Fig. 14 Localization errors in *x* , *y* and *z* axis directions caused by different detection pixel errors.

Table 7 RMSE with EKF at each axis of actual landing experiments and FPS before and after PointRefine-Net.

Index	Algorithm	*x* (m)	*y* (m)	*z* (m)	Processing rate (fps)
T2	BL-N without PR-N	0.2456	1.8082	0.1213	500.23±2.21
	BL-N with PR-N	0.2323	1.6002	0.1156	450.32±2.34

6. Concluding remarks

In this paper, a novel cascaded deep learning detection model has been proposed and developed for autonomous landing of unmanned fixed-wing aerial vehicles. A light-weight deep learning model enables a higher processing speed and makes the reasonable check and further optimization of UAV coordinates a reality. Flight experiment results validate that the approach attaches ~500 fps and higher positioning accuracy than previous work. By making full use of the expansibility of the ground computing resources, we promote the visual guidance landing system to be practical.

In the subsequent work, the developed algorithm is potentially extended to enabling detection and localization based on multiple key areas and key points.

This algorithm is also to be developed from vision-based position to pose (position-and-attitude) during the autolanding. In details, multiple anchors are to be detected simultaneously to support pose estimation then.

Acknowledgment

This study was supported by the National Natural Science Foundation of China (No. 61973327).

References

1. Kumar V, Michael N. Opportunities and challenges with autonomous micro aerial vehicles. *The International Journal of Robotics Research* 2012; 31(11):1279-91.
2. Kendoul F. Survey of advances in guidance, navigation, and control of unmanned rotorcraft systems. *Journal of Field Robotics* 2012; 29(2):315-78.
3. Tang D, Hu T, Shen L, et al. Ground stereo vision-based navigation for autonomous take-off and landing of UAVs: A Chan-Vese model approach. *International Journal of Advanced Robotic Systems* 2016; 13(2):67.
4. Gui Y, Guo P, Zhang H, et al. Airborne vision-based navigation method for UAV accuracy landing using infrared lamps. *Journal of Intelligent & Robotic Systems* 2013; 72(2):197-218.
5. Bourquardez O, Chaumette F. Visual servoing of an airplane for auto-landing. *2007 IEEE/RSJ international conference on intelligent robots and systems*; 2007 Oct 29-Nov 2; San Diego, USA. Piscataway: IEEE Press; 2007.p.1314-9.
6. Yang XY, Zhu RD, Wang JK, et al. Real-time object tracking via least squares transformation in spatial and Fourier domains for unmanned aerial vehicles. *Chinese Journal of Aeronautics* 2019; 32(7):1716-26.
7. Zhou H, Zhang T. A vision-based navigation approach with multiple radial shape marks for indoor aircraft locating. *Chinese Journal of Aeronautics* 2014; 27(1):76-84.
8. Yang T, Li G, Li J, et al. A ground-based near infrared camera array system for UAV auto-landing in GPS-denied environment. *Sensors* 2016; 16(9): 1393.
9. Santos NP, Lobo V, Bernardino A. AUTOLAND project: Fixed-wing UAV landing on a fast patrol boat using computer vision. *OCEANS 2019 MTS/IEEE SEATTLE*; 2019 Oct 27-31; Seattle, USA. Piscataway: IEEE Press; 2019.p.1-5.
10. Kong W, Zhang D, Wang X, et al. Autonomous landing of an UAV with a ground-based actuated infrared stereo vision system. *2013 IEEE/RSJ international conference on intelligent robots and systems*; 2013 Nov 3-7; Tokyo, Japan. Piscataway: IEEE Press; 2013.p. 2963-70
11. Hu T, Zhao B, Tang D, et al. ROS-based ground stereo vision detection: Implementation and experiments. *Robotics and biomimetics*; 2016 Dec 5-8; Macau SAR, China. Berlin: Springer; 2016.p.14.
12. Ma Z, Hu T, Shen L. Stereo vision guiding for the autonomous landing of fixed-wing UAVs: A saliency-inspired approach. *International Journal of Advanced Robotic Systems* 2016; 13(2):43.
13. Cao Z, Zhao K, Fang Q, et al. Enabling~ 100fps detection on a landing unmanned aircraft for its on-ground vision-based recovery. *2017 18th International Conference on Advanced Robotics (ICAR)*; 2017 Jul 10-12; Hong Kong, China. Piscataway: IEEE Press; 2017.p.407-11.
14. Tang D, Hu T, Shen L, et al. Chan-Vese model based binocular visual object extraction for UAV autonomous take-off and landing. *2015 5th International Conference on Information Science and Technology (ICIST)*; 2015 Apr 24-26; Changsha, China. Piscataway: IEEE Press; 2015.p.67-73.
15. Kong W, Zhou D, Zhang Y, et al. A ground-based optical system for autonomous landing of a fixed wing UAV. 2*014 IEEE/RSJ international conference on intelligent robots and systems*; 2014 Sep 14-18; Chicago, USA. Piscataway: IEEE Press; 2014.p.4797-804.
16. Daibing Z, Xun W, Weiwei K. Autonomous control of running takeoff and landing for a fixed-wing unmanned aerial vehicle. *2012 12th International Conference on Control Automation Robotics & Vision (ICARCV)*; 2012 Dec 5-7; Guangzhou, China. Piscataway: IEEE Press; 2012.p.990-4.
17. Chengping Y, Lincheng S, Dianle Z, et al. A new calibration method for vision system using differential GPS. *2014 13th International Conference on Control Automation Robotics & Vision (ICARCV)*; 2014 Dec 10-12; Singapore, Singapore. Piscataway: IEEE Press; 2014.p.1514-7.
18. Zhang Y, Shen L, Cong Y, et al. Ground-based visual guidance in autonomous UAV landing. *Sixth International Conference on Machine Vision (ICMV 2013)*; London, UK. Bellingham: SPIE; 2013.p. 90671W.
19. Ren S, He K, Girshick R, et al. Faster R-CNN: Towards real-time object detection with region proposal networks. *Advances in neural information processing systems*; 2015 Dec 7-12; Montreal, Canada. New York: ACM; 2015.p. 91-9.
20. Redmon J, Farhadi A. YOLOv3: An incremental improvement[Internet]. 2018 Apr [cited 2020 May 15]; Available from:

https://arxiv.org/abs/1804.02767.
21. Huang G, Liu Z, Van Der Maaten L, et al. Densely connected convolutional networks. *Proceedings of the IEEE conference on computer vision and pattern recognition*; 2017 Jul 21-26; Hawaii, USA. Piscataway: IEEE Press; 2017. p.4700-8.
22. Sun K, Xiao B, Liu D, et al. Deep high-resolution representation learning for human pose estimation. *Proceedings of the IEEE conference on computer vision and pattern recognition*; 2019 Jun 16-20; Los Angeles, USA. Piscataway: IEEE Press; 2019.p.5693-703.
23. Lin T-Y, Maire M, Belongie S, et al. Microsoft coco: Common objects in context. *European conference on computer vision*; 2014 Sep 6-12; Zurich, Switzerland. Berlin: Springer; 2014.p.740-55.
24. Deng J, Dong W, Socher R, et al. Imagenet: A large-scale hierarchical image database. *2009 IEEE conference on computer vision and pattern recognition*; 2009 Jun 20-25; Florida, USA. Piscataway: IEEE Press; 2009. p.248-55.
25. Everingham M, Van Gool L, Williams CK, et al. The pascal visual object classes (VOC) challenge. *International Journal of Computer Vision* 2010; 88(2):303-38.
26. Tang X, Yang W, Hu X, et al. A novel simplified model for torsional vibration analysis of a series-parallel hybrid electric vehicle. *Mechanical Systems and Signal Processing* 2017; 85:329-38.
27. Newell A, Yang K, Deng J. Stacked hourglass networks for human pose estimation. *European conference on computer vision*; 2016 Oct 8-16; Amsterdam, Netherlands. Berlin: Springer; 2016.p.483-99.
28. Redmon J, Farhadi A. YOLO9000: Better, faster, stronger. *Proceedings of the IEEE conference on computer vision and pattern recognition*; 2017 Jul 21-26; Hawaii, USA. Piscataway: IEEE Press; 2017.p.7263-71.
29. Howard AG, Zhu M, Chen B, et al. Mobilenets: Efficient convolutional neural networks for mobile vision applications[Internet]. 2017 Apr [cited 2020 May 15]; Available from: https://arxiv.org/abs/1704.04861.
30. Liu W, Anguelov D, Erhan D, et al. SSD: Single shot multibox detector. *European conference on computer vision*; 2016 Oct 8-16; Amsterdam, Netherlands. Berlin: Springer; 2016.p.21-37.